

TOPOGRAPHIC RESPONSE TO HIGH WAVES AND SUBSEQUENT BEACH RECOVERY ON CHIGASAKI COAST

Takahisa Tamura¹, Toshinori Ishikawa², Takaaki Uda³ and Masumi Serizawa⁴

Beach topography quickly responds to the action of storm waves, resulting in foreshore erosion and accretion under calm wave conditions after a storm. Field observations were carried out on the Chigasaki coast to investigate these beach changes. It was found that the seabed shallower than 3 m depth was rapidly eroded by offshore sand transport during a storm event with the deposition of sand in a zone at depths between 3 and 5 m, and then the beach recovered within 1–2 years after the storm. Topographic changes immediately after the storm and subsequent recovery under calm wave conditions were calculated using the BG model (a model for predicting three-dimensional beach changes based on Bagnold's concept). Given the equilibrium slope of fine sand d_1 and medium-size sand d_2 to be 1/120 during high waves, the erosion of the foreshore zone was numerically reproduced. Moreover, the recovery of the beach topography to a gentle slope under calm wave conditions after the storm was successfully reproduced.

Keywords: offshore sand transport; beach cycle; BG model; Chigasaki coast

INTRODUCTION

Beach topography quickly responds to the action of storm waves, resulting in foreshore erosion and accretion under calm wave conditions after a storm event. Davis and Fitzgerald (2004) clarified these beach cycles; when wave conditions are about equal to or less than the average energy conditions, such as a swell wave with a small wave height of generally less than 1 m and a period of 8–12 s, an accretionary beach is formed together with another condition of an erosive or storm beach. These beach changes may occur on beaches with protective measures or artificial beaches produced by beach nourishment. On these beaches, the shore protection function of a sandy beach is reduced when a trough is formed immediately offshore of the shoreline, because the wave run-up height increases with the increase in the foreshore slope. It is necessary, therefore, to predict these beach changes at the planning stage of an artificial beach. In this study, these topographic changes due to high waves and subsequent beach recovery under calm wave conditions were calculated using the BG model (a model for predicting 3-D beach changes based on Bagnold's concept; Uda et al., 2018), taking the Chigasaki coast in Kanagawa Prefecture, Japan, as an example.

COASTAL CONDITIONS OF STUDY AREA

The study area is the Chigasaki coast located 1 km east of the Sagami River mouth (Fig. 1). This coast has been formed through the deposition of sand supplied from the Sagami River and transported by eastward longshore sand transport. The beach, however, has been eroded owing to the decrease in the amount of fluvial sand supplied from the Sagami River and the blockage of eastward longshore sand transport by the construction of Chigasaki fishing port. As a measure against beach erosion, an artificial headland was constructed 1.4 km east of the fishing port in 1990, and beach nourishment using material composed of sand and gravel with grain sizes greater than those of the original seabed material has been carried out at a rate of 3×10^4 m³/yr between the fishing port and the artificial headland since 2005. As a result, the shoreline has markedly recovered by 2022 (Fig. 2). However, storm waves of the largest level in observation history hit this coast several times, associated with typhoons, causing erosion of the foreshore formed by beach nourishment and the collapse of the cycling road along the coastline. On this coast, the foreshore mainly composed of gravel was relatively stable during storms, but the nearshore zone was severely eroded, resulting in sand deposition in the offshore area. Ishikawa et al. (2020) clarified that the foreshore was eroded owing to the rapid offshore sand transport during a storm event with the deposition of sand in a zone at depths between 3 and 5 m, and the beach recovered within 1–2 years after the storm event.

¹ Kanagawa Prefectural Government, 1 Nihon-Odori, Naka-ku, Yokohama, Kanagawa 231-8588, Japan

² Chuo University, 1-13-27 Kasuga, Bunkyo-ku, Tokyo 112-8551, Japan

³ Public Works Research Center and Nihon University, 1-6-4 Taito, Taito-ku, Tokyo 110-0016, Japan

⁴ Coastal Engineering Laboratory Co., Ltd., 1-22-301 Wakaba, Shinjuku-ku, Tokyo 160-0011, Japan



Figure 1. Satellite image of the Chigasaki coast.



Figure 2. Beach conditions in 2005 and 2022 before and after beach nourishment, respectively.

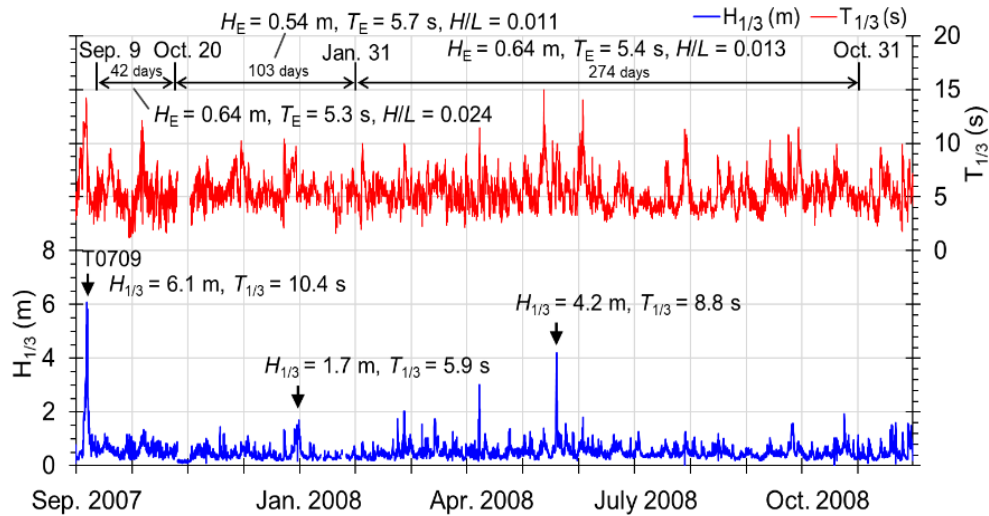
TOPOGRAPHIC CHANGES IMMEDIATELY AFTER STORM EVENTS AND RECOVERY AFTER STORMS

In recent years, storm waves of the largest level in observation history, associated with typhoons, hit this coast several times. During Typhoon No. 9 in 2007 (T0709) and T1721, which hit the coast on 6 September 2007 and 23 October 2017, respectively, rough waves with significant wave heights of $H_{1/3} = 6.1$ m ($T_{1/3} = 10.4$ s) and 7.1 m ($T_{1/3} = 11.2$ s) were measured at a 20 m depth of the Hiratsuka wave observatory 4.7 km west of the fishing port, as shown in Fig. 3, causing significant offshore sand transport. Thereafter, relatively calm wave conditions prevailed, although storm waves with significant wave heights greater than 4 m ($H_{1/3} = 4.38$ m and 5.66 m) were measured on 11 December 2017 and 1 October 2018, respectively, after T1721.

To monitor the topographic changes of this coast, seabed topographies were measured by Narrow Multi-Beam surveys. Figure 4(a) shows the planar distribution of topographic changes between February 2007 before T0709 and January 2008 measured four months after the typhoon. A trough was formed in a zone between -2 and -3 m owing to the offshore sand movement induced by storm waves, and sand was deposited in a zone between -3 and -5 m. Then, erosion occurred in a zone between -3 and -4 m, and sand was deposited near the shoreline owing to the shoreward sand transport between January 2008 and February 2009, as shown in Fig. 4(b).

Figure 5 shows the change in the longitudinal profile along transect No. 18 crossing the central part of the coast, as shown in Fig. 4. In March 2007 before T0709, the profile had a step near -2 m and the slope between -2 and -6 m was $1/37$. However, by October 2007 after T0709, the zone between -2 and -3 m was eroded and sand was transported offshore, forming a bar at a depth of -3.4 m and the slope became gentle from $1/37$ to $1/45$ in a zone between -2 and -6 m. Then, shoreward sand transport occurred and the bar depth decreased to up to -2.8 m by January 2008. During this period, the energy-mean significant wave height, period, and wave steepness were $H_E = 0.54$ m, $T_E = 5.7$ s, and $H/L = 0.011$, and the maximum significant wave height and corresponding wave period were $H_{1/3} = 1.7$ m and $T_{1/3} = 5.4$ s, respectively, as shown in Fig. 3(a). Although the trough remained as it was until January 2008, the trough was refilled by October 2008 owing to shoreward sand transport and the seabed slope between -2 and -6 m returned from $1/45$ to $1/37$. During this period, the energy-mean significant wave height, period, and wave steepness were almost the same as those in the preceding period: $H_E = 0.64$ m, $T_E = 5.4$ s, and $H/L = 0.013$, respectively. Thus, the beach profile returned to the original one through the action of calm waves after the storm, and the duration necessary for this recovery was one year between October 2007 and October 2008.

(a) T0709 hit on 6 September 2007



(b) T1721 hit on 23 October 2017

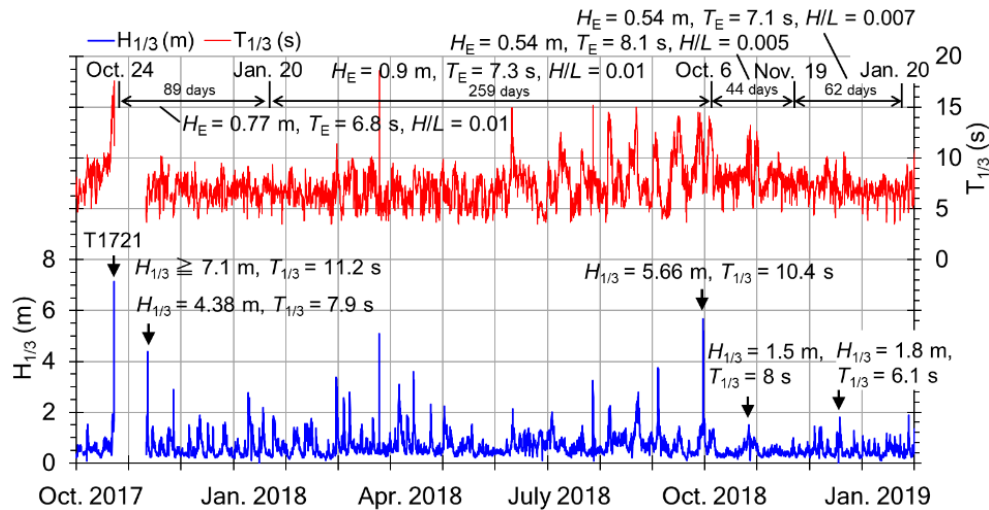
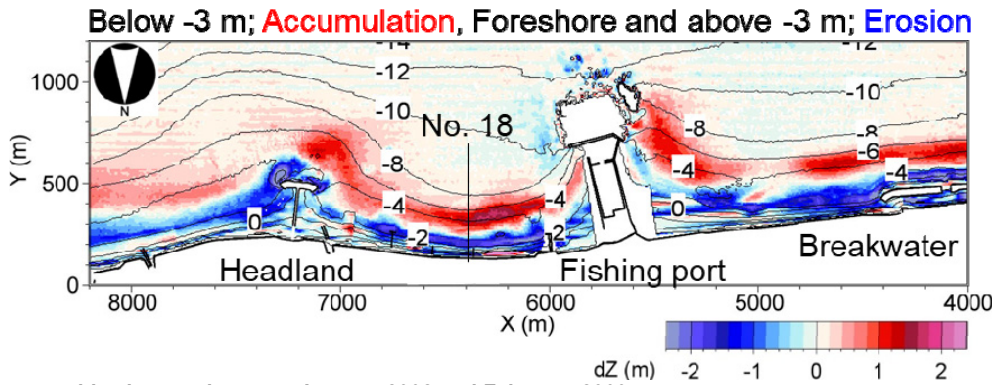


Figure 3. Changes in significant wave height and period during T0709 and T1721 measured at Hiratsuka wave observatory.

Similarly, Fig. 6(a) shows the topographic changes between December 2016 before T1721 and January 2018, approximately 3 months after T1721. A rapid beach erosion occurred in a zone shallower than -3 m with deposition of sand in a zone between -3 and -4 m, similarly to the beach changes that occurred in T0709. Moreover, Fig. 6(b) shows the topographic changes between January 2018 and January 2019, approximately 15 months after T1721. Similar to the effect of T0709, the beach was eroded in a zone between -3 and -4 m and sand was deposited near the shoreline.

Figure 7 shows the changes in the longitudinal profile along transect No. 18. The beach profile had a step at -2 m and the seabed slope in a zone between -2 and -6 m was $1/25$ on 6 September 2017 before T1721. By 20 January 2018, 89 days after T1721, a bar with a crown depth of 3.2 m was formed owing to the seaward sand transport associated with storm waves, and the seabed slope between -2 and -6 m became $1/40$. Then, shoreward sand transport occurred with the trough being buried by 19 November, and the longitudinal profile of a gentle slope completely recovered and the seabed slope in a zone between -2 and -6 m became $1/34$ by 20 January 2019, which was 454 days after T1721. It was concluded that although a bar and trough were formed immediately after T1721, a gentle slope topography was formed again after 454 days. This topographic recovery was mainly triggered by the shoreward sand transport under calm wave conditions with $H_{1/3} = 0.81$ m, $T_{1/3} = 7.3$ s, and $H/L = 0.009$ prevailed during this period (Fig. 3).

(a) Topographic changes between February 2007 and January 2008



(b) Topographic changes between January 2008 and February 2009

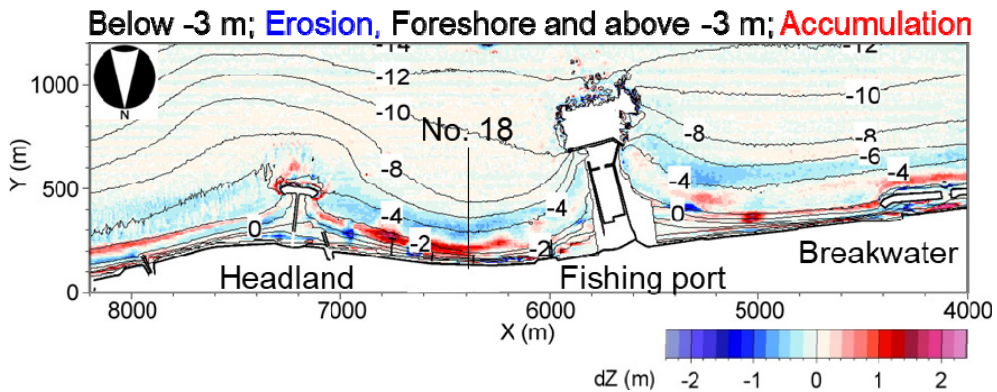


Figure 4. Topographic changes between February 2007 and January 2008, and between January 2008 and January 2009.

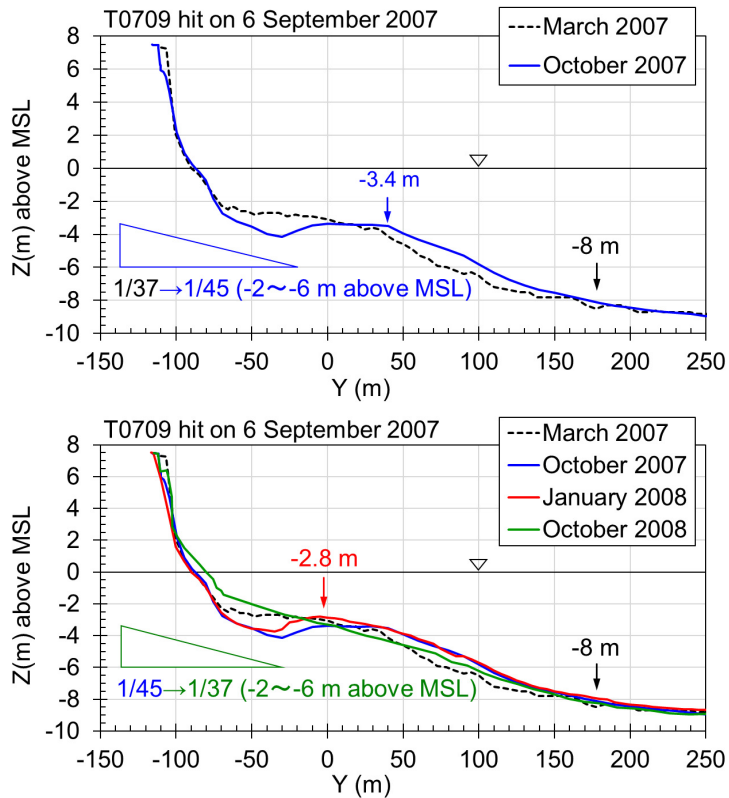
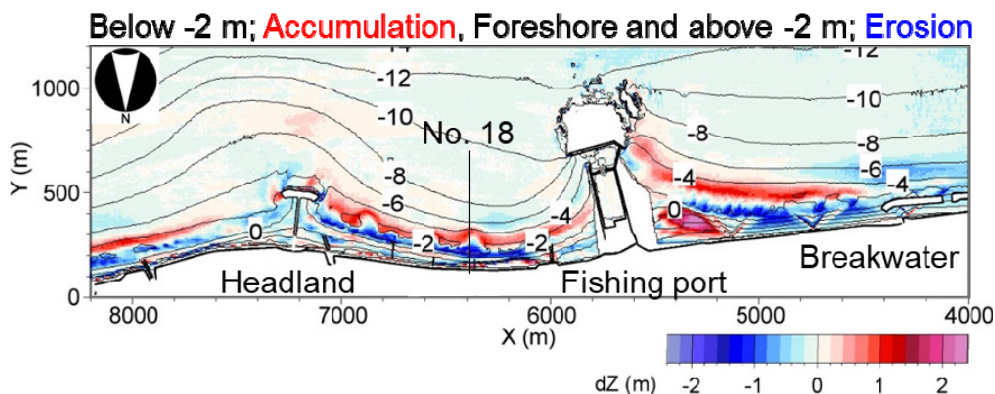


Figure 5. Changes in longitudinal profile along transect No. 18 after T0709.

(a) Topographic changes between December 2016 and January 2018



(b) Topographic changes between January 2018 and January 2019

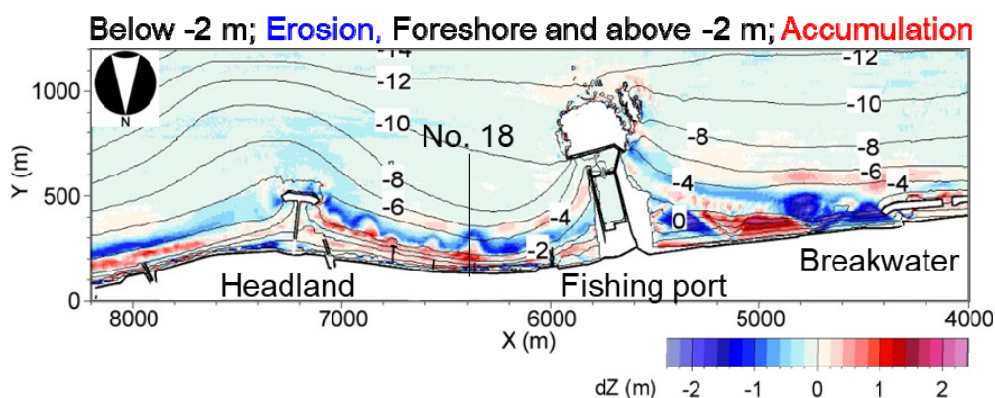


Figure 6. Topographic changes between December 2016 and January 2018, and between January 2018 and January 2019.

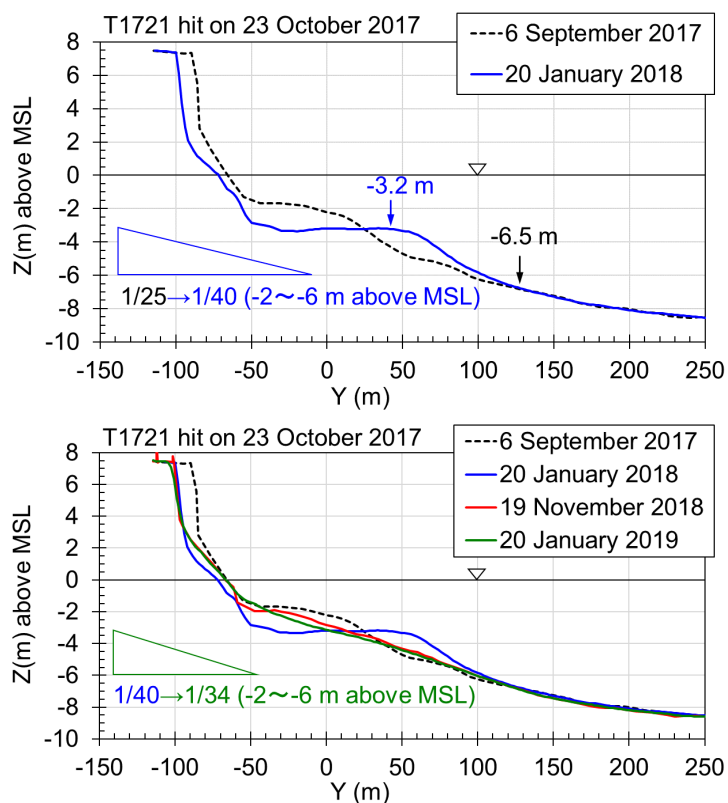


Figure 7. Changes in longitudinal profile along transect No. 18 after T1721.

Figure 8 shows the depth distribution of the content of the seabed material along transect No. 18. The seabed material was mostly composed of fine and medium-size sand, although the gravel content was as high as 60–70% in a zone between -1 and -2 m in September 2017 before T1721, whereas coarse material composed of gravel remained near -1 m and the gravel content increased on the foreshore until November 2017 immediately after the typhoon. Although a bar was formed in the zone between -3 and -5 m after T1721, as shown in Fig. 5, the grain size composition at depth of -4 m was 7% gravel, 8% coarse sand, 57% medium-size sand, and 28% fine sand. Then, until November 2018 when a bar was eroded and a trough was refilled, the composition became 0% gravel, 1% coarse sand, 52% medium-size sand, and 45% fine sand, and thus, the contents of gravel, coarse sand, and medium-size sand decreased, whereas the content of fine sand increased, as the grain size composition recovered to that before T1721. From these findings, it was concluded that medium-size sand was mainly transported offshore and deposited, forming a bar during a storm event.

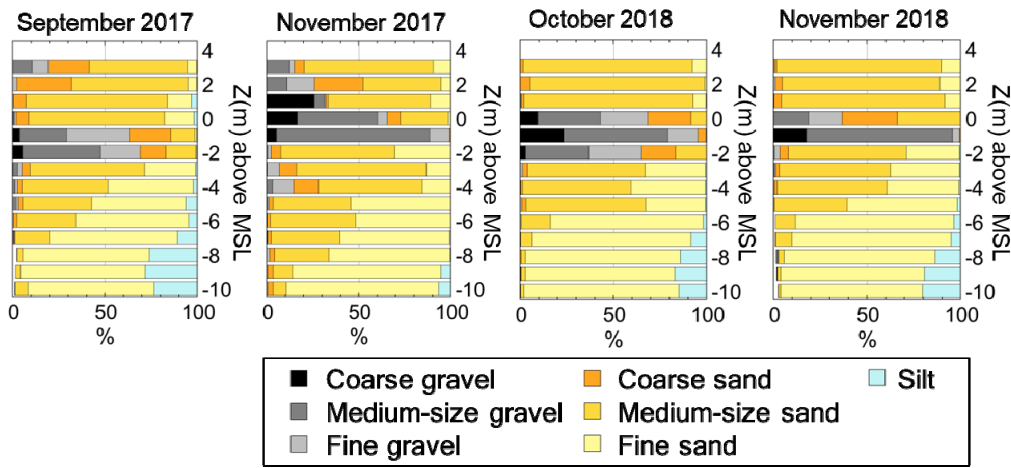


Figure 8. Depth distribution of contents of bed material along transect No. 18.

REPRODUCTION OF TOPOGRAPHIC CHANGES USING BG MODEL

Calculation Method

To predict the topographic changes induced by waves, a concept of the change in equilibrium slope in response to the change in wave intensity was introduced by Fukuhama et al. (2008). They proposed a model for predicting the change in the longitudinal profile under the action of storm waves and subsequent calm waves by assuming that the equilibrium slope of the seabed composed of a certain grain size changes in response to the wave intensity. The same concept was incorporated into the contour-line-change model proposed by Serizawa et al. (2003), which successfully simulated rapid beach changes caused by storm waves and subsequent beach recovery due to calm waves after a storm on the Seisho coast (Serizawa et al., 2009).

Figure 9 shows a schematic diagram of this concept (Fukuhama et al., 2008). When the longitudinal slope is equal to the equilibrium slope under mean waves, the longitudinal profile is stable with no beach changes (Fig. 9(a)). When the wave height decreases, the equilibrium slope becomes steeper, and as a result, the restoring force may occur for the equilibrium slope to be restored, causing shoreward sand transport (Fig. 9(b)). Conversely, when the wave height increases, the equilibrium slope becomes gentle, resulting in seaward sand transport (Fig. 9(c)). Thus, the change in the longitudinal profile could be expressed by the change in the beach slope in response to wave intensity. In this study, we follow this concept.

Out of storm waves that hit the Chigasaki coast since 2007, those generated by Typhoon No. 21 (T1721), which hit the coast in October 2017, were adopted as a typical case, and reproduction calculations of rapid beach changes due to the offshore sand transport triggered by storm waves were carried out in Case 1 and the recovery of the beach topography under calm wave conditions were carried out in Case 2. Although high waves greater than $H_{1/3} = 7.1$ m with $T_{1/3} = 11.2$ s were incident during T1721, as shown in Fig. 3(b), and relatively calm wave conditions prevailed, except for high waves of $H_{1/3} = 4.38$ m on 11 November 2017 and $H_{1/3} = 5.66$ m on 1 October 2018. On 6 September

2017 before T1721, a step with a depth of approximately 2 m was formed offshore of the shoreline, as shown in Fig. 5. However, this step and nourishment mound were eroded away owing to seaward sand transport under storm wave conditions. On 20 January 2018, 89 days after the storm event, a large bar was formed at a depth of 3.2 m. Although a trough remained as it was, the trough was filled with sand by 19 November 2018. Furthermore, by 20 January 2019, the longitudinal profile recovered to the original one before the typhoon. Thus, the topography requires over one year to recover, and the energy mean wave height and period were $H_{1/3} = 0.81$ m and $T_{1/3} = 7.3$ s, respectively.

For the calculation of the wave field, the energy balance equation method (Mase, 2001) was employed, and the calculation domain with a 4.7 km length alongshore and 2.7 km length in the cross-shore direction, as shown in Fig. 10, was adopted. The topographic changes owing to high waves and subsequent beach recovery under the calm wave conditions were calculated using the BG model. The calculation domain for topographic changes was 2 km alongshore and 1.2 km in the cross-shore direction, as shown in Fig. 11.

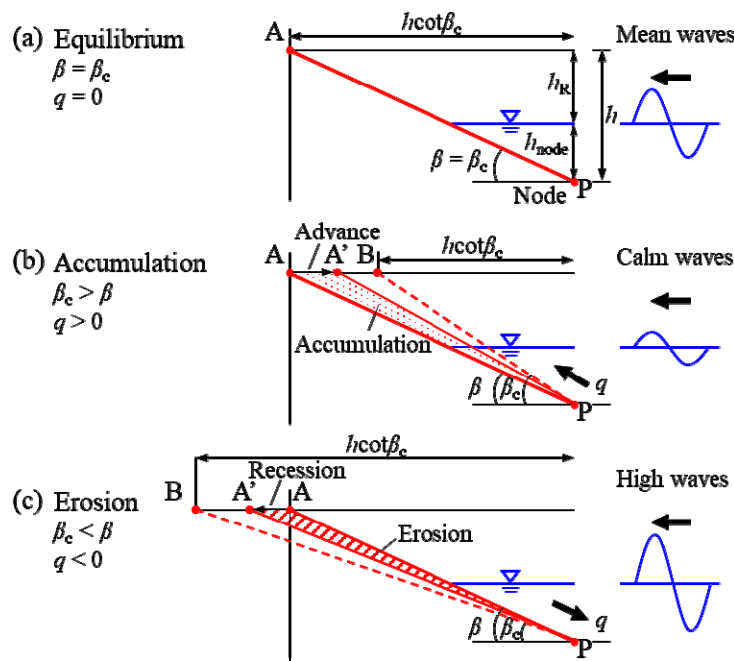


Figure 9. Schematic diagram of the changes in foreshore slope and shoreline position under the concept of equilibrium slope (Fukuhama et al., 2008).

Calculation conditions

The topographic changes including the rapid beach erosion by high waves during a storm event and the recovery after 89 and 454 days from this event were calculated using the BG model. In this calculation, the beach material was assumed to be composed of five grain sizes on the basis of the longitudinal profile and the depth distribution of the grain sizes of the seabed material, as shown in Fig. 12: fine sand (d_1), medium-size sand (d_2), coarse sand (d_3), and fine and medium-size gravel (d_4). Fine sand (d_1) mainly deposited in a zone deeper than -7 m, medium-size sand (d_2) deposited in a zone shallower than -6 m except for the vicinity of the shoreline, and coarse sand (d_3) deposited near the shoreline.

The equilibrium slopes corresponding to the grain sizes were assumed to be $1/40$ (d_1), $1/25$ (d_2), and $1/10$ (d_3). On the other hand, because fine and medium-size gravel (d_4) and coarse gravel (d_5) were contained in the beach nourishment material, the material was assumed to be a mixture of 16.5% fine sand (d_1), 29.8% medium-size sand (d_2), 11.3% coarse sand (d_3), 25.5% fine and medium-size gravel (d_4), and 9.9% (d_5) coarse gravel on the basis of the compositions measured each year (Fig. 13). Moreover, the equilibrium slopes corresponding to the grain sizes d_4 and d_5 were assumed to be $1/8$ and $1/5$, respectively, as reported by Ishikawa et al. (2018).

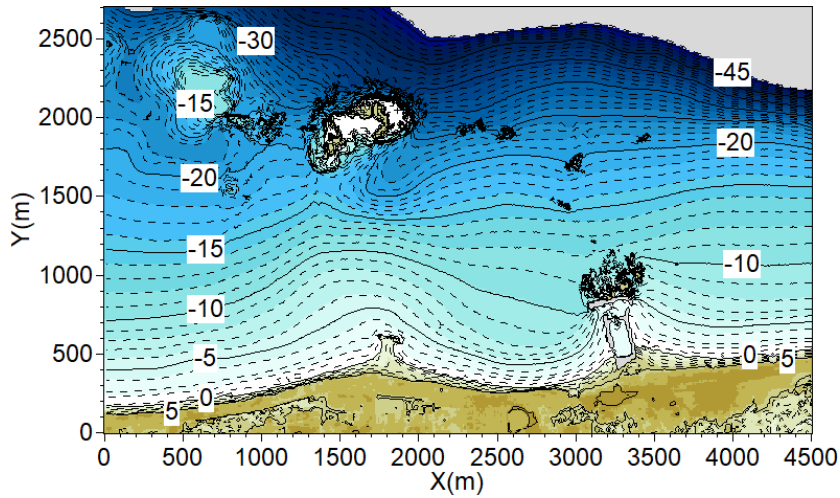


Figure 10. Calculation domain of wave field.

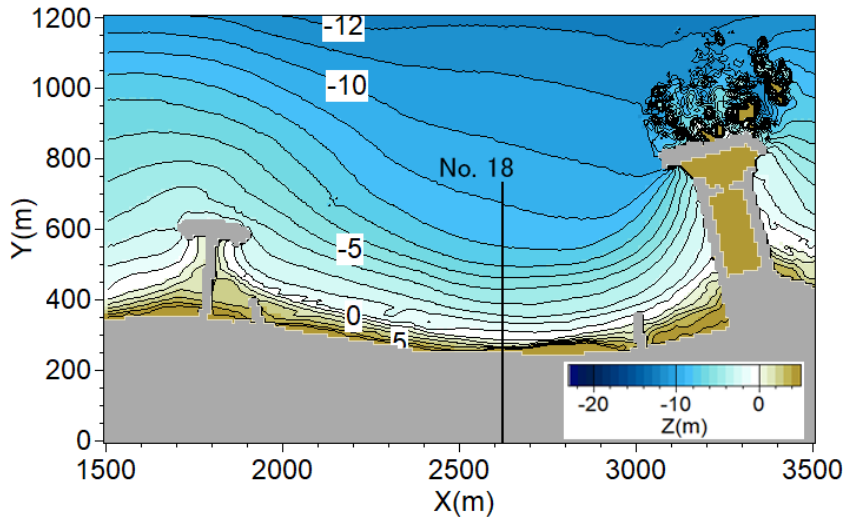


Figure 11. Calculation domain of topographic changes.

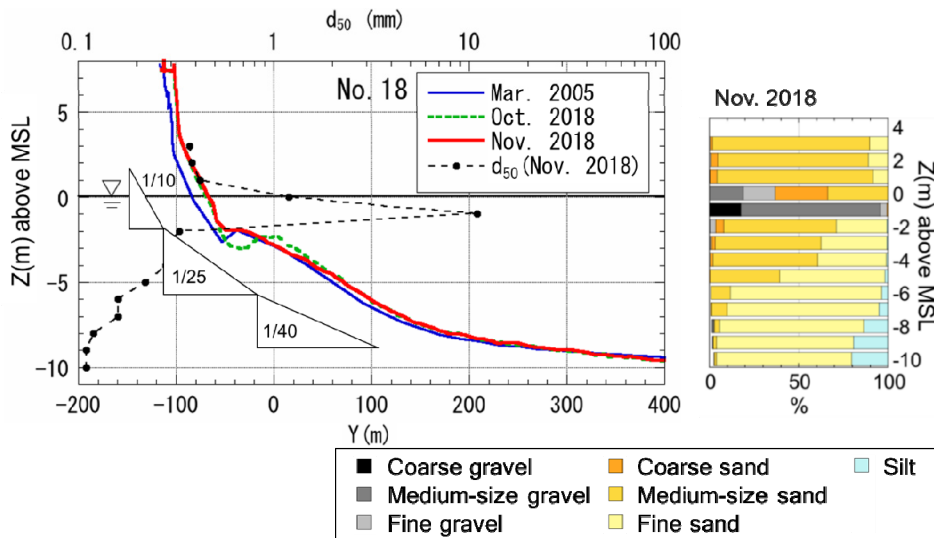


Figure 12. Longitudinal profile along transect No. 18 and depth distribution of grain sizes of bed material.

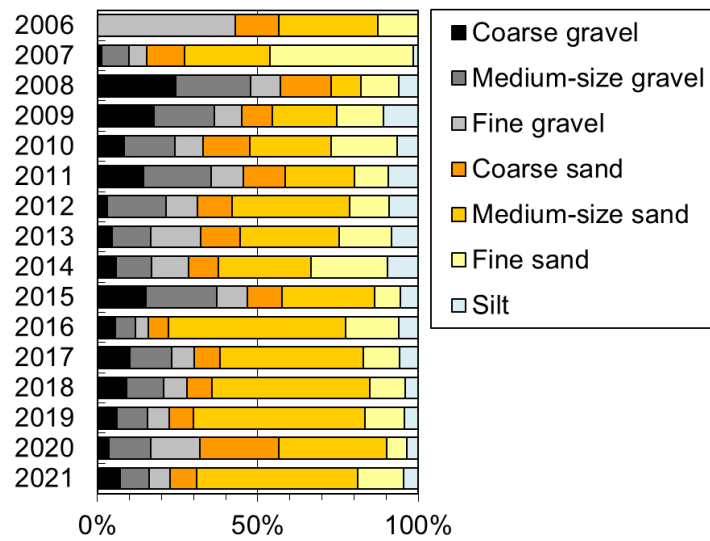


Figure 13. Contents of each grain size in beach nourishment material.

The initial topography in a zone shallower than -8 m was determined from the measured data in the NMB survey in December 2016, whereas the seabed in a zone deeper than -8 m was assumed to be a solid bed. For the initial grain size distribution, the seabed is assumed to be fully filled with grains of sizes d_3 , d_2 , and d_1 in a zone shallower than -1 m, the zone between -1 and -7 m, and a zone deeper than -7 m, respectively.

For the wave conditions in Case 1, high waves during the storm event were set to be $H_{1/3} = 7.1$ m and $T_{1/3} = 11.2$ s, as observed on 23 October 2017 at the Hiratsuka wave observatory during T1721 together with the wave incidence angle of $N175^\circ E$ (Fig. 2(b)). Moreover, the wave conditions during the subsequent beach recovery in Case 2 were set to be the energy mean wave height $H_{1/3} = 0.81$ m and the wave period $T_{1/3} = 7.3$ s measured over 454 days between 24 October 2017 and 20 January 2019 together with the wave direction of $176^\circ E$.

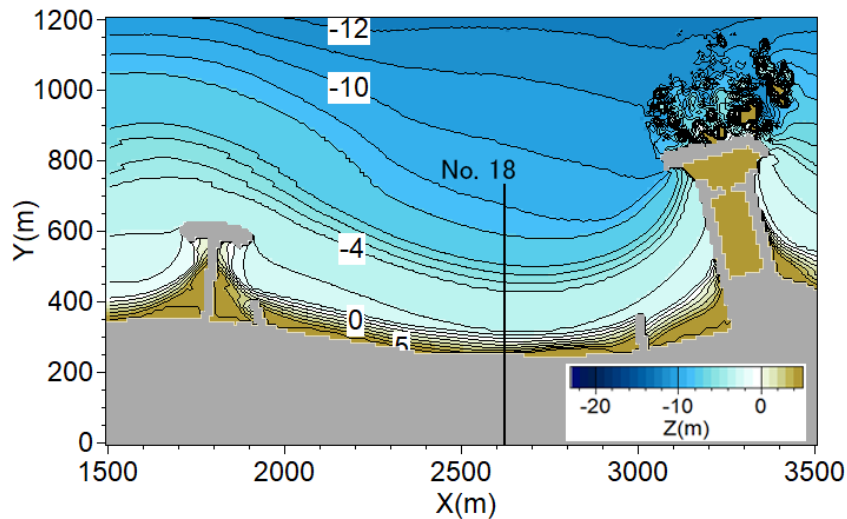
In Case 1, the time interval was set to be $\Delta t = 10^{-4}$ h/step and the duration was 12 h on the basis of the observed duration of rough waves during the typhoon, which can be characterized by the duration of waves with the significant wave height of over 2 m. The berm height and the sand transport coefficient A were set to be $h_R = 5$ m and 0.3, respectively. Similarly, in Case 2, the time interval was set to be $\Delta t = 5 \times 10^{-2}$ h/step and the duration time was 454 days. The berm height was set to be $h_R = 3$ m because of the reduction in incident wave height and the sand transport coefficient A to be 0.07. Regarding the depth of closure h_c , a constant value of 8 m was employed in both calculations in Cases 1 and 2, because h_c took a constant value of 8 m because of no changes in longitudinal profile, as shown in Fig. 4. The change in the equilibrium slope in response to the change in wave height was empirically determined to be $\tan\beta_1 = \tan\beta_2 = 1/120$ under storm wave conditions on the basis of the profile changes. For the recovery process of the profile, the original slope before the erosion was assumed to recover, such as $\tan\beta_1 = 1/40$ and $\tan\beta_2 = 1/25$ under energy mean wave conditions. These calculation conditions are summarized in Table 1.

Table 1. Calculation conditions.	
Calculation cases	Case 1: Calculation of topographic changes induced by storm waves during T1721 between 21 October 2017 and 24 October 2017 Case 2: Calculation of recovery process of topography under calm wave conditions from immediately after storm event to 20 January 2018 (89 days) and 20 January 2019 (454 days)
Initial topography	Case 1: Seabed topography measured by NMB survey in December 2016 Case 2: Calculation results in Case 1
Calculation duration	0.5d (12 h) in Case 1 and 454 days (15 months) in Case 2
Wave conditions	Case 1: $H_{1/3} = 7.1$ m, $T_{1/3} = 11.2$ s, wave direction N175°E (maximum wave height measured at Hiratsuka wave observatory during T1721) Case 2: $H_E = 0.81$ m, $T_E = 7.3$ s, wave direction N176°E (energy mean waves in recovery process of beach between 24 October 2017 and 20 January 2019)
Tide level	Mean sea level
Mesh size	$\Delta X = 10$ m
Time intervals	Case 1: $\Delta t = 10^{-4}$ h/step, Case 2: 5×10^{-2} h/step
Grain size and equilibrium slopes	Fine sand ($d_1 = 0.075\text{--}0.15$ mm, typical grain size $d = 0.15$ mm), $\tan\beta_1 = 1/40$ Medium-size sand ($d_2 = 0.15\text{--}0.85$ mm, $d = 0.20$ mm), $\tan\beta_2 = 1/25$ Coarse sand ($d_3 = 0.85\text{--}2$ mm, $d = 1.0$ mm), $\tan\beta_3 = 1/10$ Fine and medium-size gravel ($d_4 = 2\text{--}19$ mm, $d = 4.75$ mm), $\tan\beta_4 = 1/8$ Large gravel (d_5 greater than 19 mm, $d = 19$ mm), $\tan\beta_5 = 1/5$
Changes in equilibrium slope	$\tan\beta_1 = \tan\beta_2 = 1/120$ under storm wave condition $\tan\beta_1 = 1/40$, $\tan\beta_2 = 1/25$ under energy mean wave condition
Initial content	$d_3 = 100\%$ (shallower than -1 m), $d_2 = 100\%$ (between -1 and -7 m), $d_1 = 100\%$ (deeper than -7 m)
Beach nourishment material	Mixture of 16.5% (d_1), 29.8% (d_2), 11.3% (d_3), 25.5% (d_4), and 9.9% (d_5)
Depth distribution of sand transport	Uniform
Depth of closure	$h_c = 8$ m
Berm height	$h_R = 5$ m (Case 1), $h_R = 3$ m (Case 2)
Sand transport coefficient	$A = 0.3$ (Case 1), $A = 0.07$ (Case 2), $K_y/K_z = 0.2$, $K_2 = 1.62 K_x$
Boundary conditions	Free boundary at east and west ends, and $q = 0$ at landward and seaward ends

Calculation Results

Figure 14 shows the results of the topographic changes in the reproduction calculation in Case 1 immediately after the storm event. The beach was eroded in a zone shallower than -3 m, and sand was transported offshore. Next, the recovery of the beach topography under calm wave conditions (Case 2) was carried out under the conditions that the energy mean waves are incident, given the topography immediately after the storm event as the initial topography. Figure 15 shows the calculation results 89 days after the storm event, which can be compared with the measured results on 19 January 2018. By comparing the topography after 89 days with that immediately after high waves, we found that the beach recovery proceeded through sand transport from the offshore zone and redeposition near the shoreline, as shown in Fig. 15(b). However, in the comparison of the initial topography and the topography after 89 days, erosion near the shoreline and accretion in the offshore zone remained and these correspond to the measured topographic changes, as shown in Fig. 4(a). Moreover, to compare the data measured on 20 January 2019 when the topography returned to that before the storm waves, the beach topography 454 days after the storm event is shown in Fig. 16. The topographic changes after 89 days compared with the topography immediately after high waves, as shown in Fig. 16(b), correspond to the results shown in Fig. 4(b). Moreover, the characteristics that the area in a zone deeper than -4 m was eroded and sand was deposited near the shoreline were well reproduced.

(a) Topography immediately after high waves



(b) Topographic changes in reference to initial topography

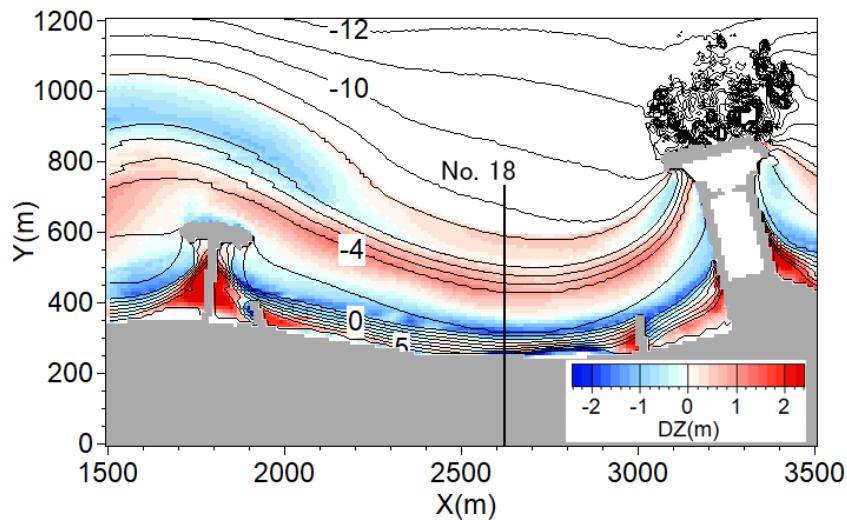
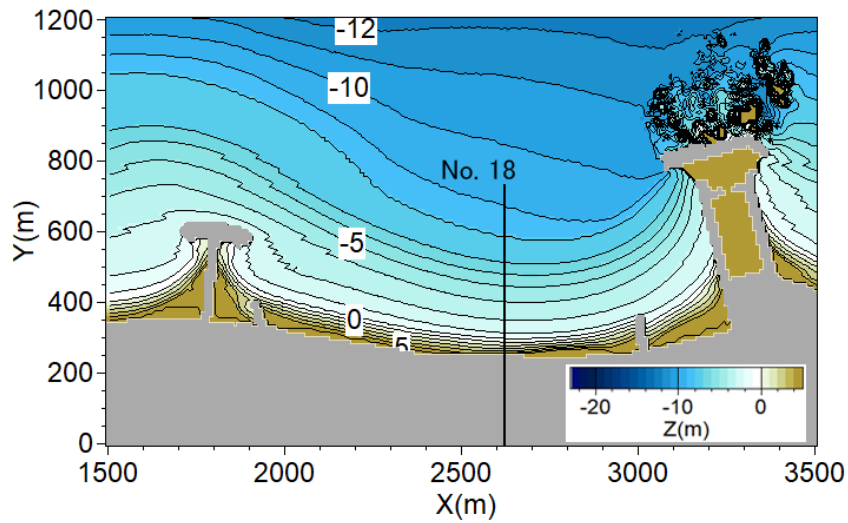
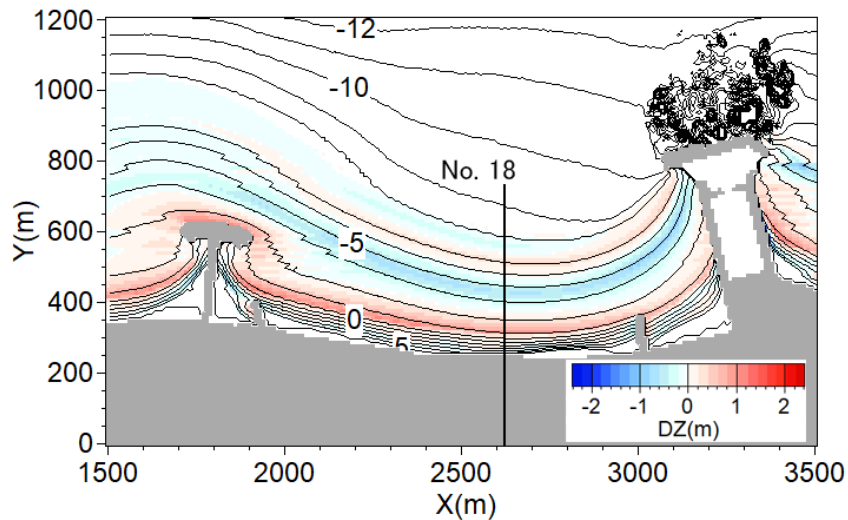


Figure 14. Calculation results in Case 1.

(a) Topography when 89 days elapsed after high waves



(b) Topographic changes in reference to topography immediately after high waves



(c) Topographic changes in reference to initial topography

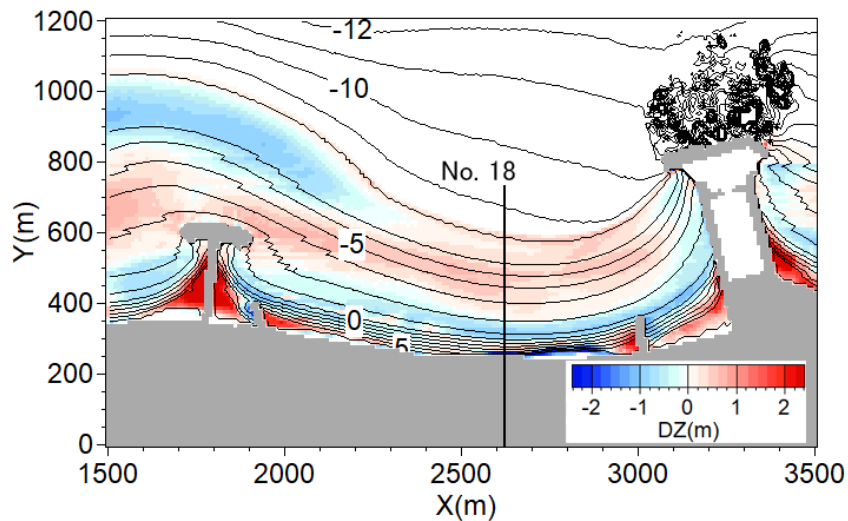
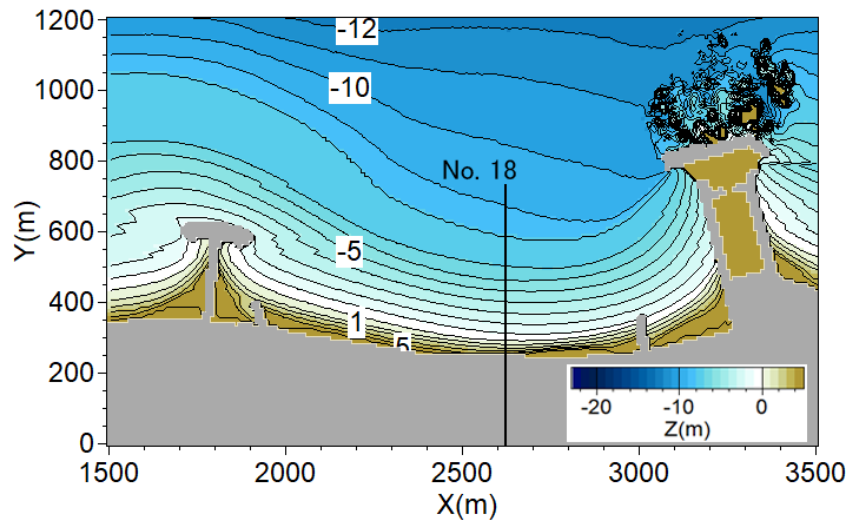


Figure 15. Calculation results in Case 2 89 days after storm event.

(a) Topography when 454 days elapsed after high waves



(b) Topographic changes in reference to topography when 89 days elapsed after high waves

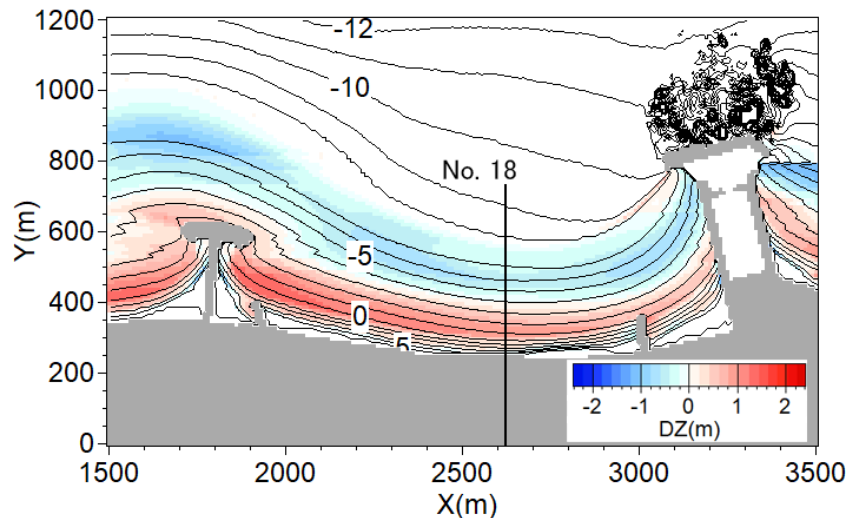


Figure 16. Calculation results in Case 2 454 days after storm event.

The changes in longitudinal profiles along transect No. 18 are shown in Fig. 17. It is found that the beach nourishment mound and the area between the shoreline and the zone of -4 m were eroded and sand was deposited in the offshore zone owing to the action of storm waves. Then, the profile gradually recovered by 89 days after the storm event, and by 454 days, the recovery of the seabed with a gentle slope was completed.

CONCLUSIONS

In this study, topographic changes immediately after the storm event and subsequent recovery under calm wave conditions were calculated using the BG model. As a result, the rapid beach erosion and the deposition of sand in the offshore zone by seaward sand transport associated with the storm waves were reproduced, given the sand transport coefficient A to be 0.3 and assuming the beach slope corresponding to the grain sizes d_1 and d_2 ($Z > -4$ m) to be $1/120$. On the other hand, the recovery process of the topography was well calculated given $A = 0.07$, which was much smaller than that under storm wave conditions, and assuming the original seabed slope of $\tan\beta_1 = 1/40$ and $\tan\beta_2 = 1/25$ under energy mean wave condition. In this study, the change in the equilibrium slope was empirically assumed on the basis of the measured slope change. In forecasting these beach changes, further studies are required.

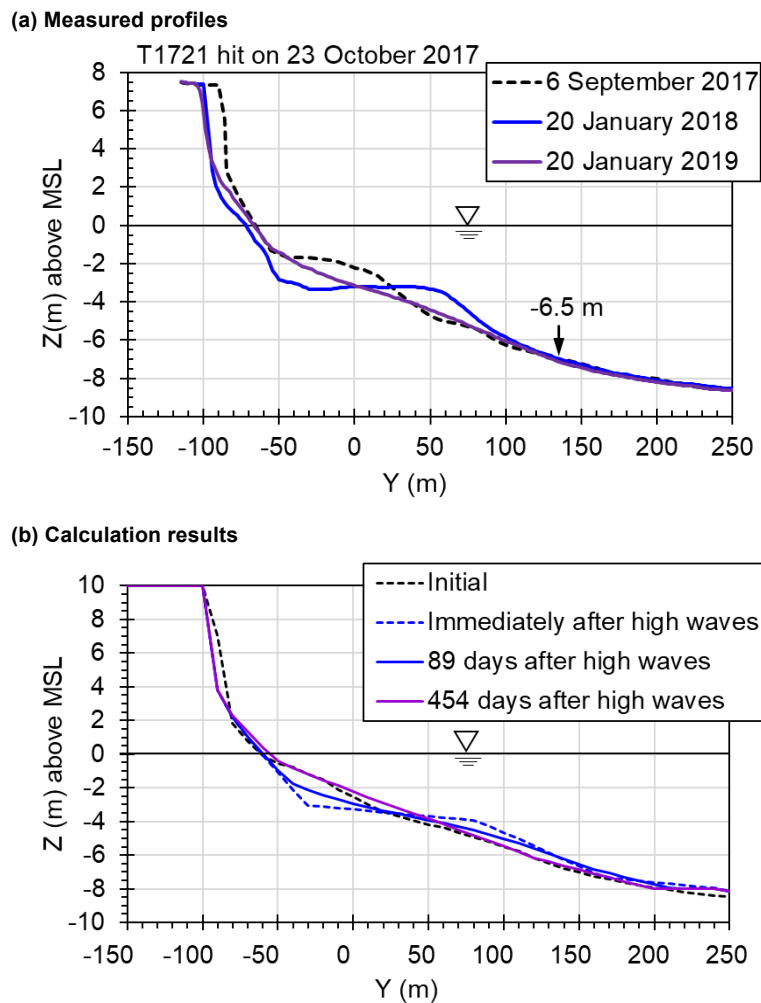


Figure 17. Changes in longitudinal profiles along transect No.18 during recovery period.

REFERENCES

- Davis Jr., R. A. and Fitzgerald, D. M. 2004. *Beaches and Coasts*, Blackwell Publishing, Malden, USA, p. 419.
- Fukuhama, M., Uda, T., Yamada, K., Serizawa, M., and Ishikawa, T. 2008. Model for predicting short-term variation of foreshore slope and shoreline applying concept of equilibrium slope, *Proc. 31st ICCE*, 1839–1850.
- Ishikawa, T., Uda, T., Furuike, K., Hosokawa, J., and Tako, T. 2018. Development of predictive model of beach changes considering not only local coast but also balance in littoral cell, *Proc. JSCE (Coastal Engineering)*, Vol. 74, No. 2, I_883–I_888. (in Japanese)
- Ishikawa, T., Uda, T., Hosokawa, J., and San-nami, T. 2020. Recovery of sandy beach after typhoon waves—Case study on Chigasaki coast, papers.42, No. 36 *vICCE*.
- Mase, H. 2001. Multidirectional random wave transformation model based on energy balance equation, *Coastal Eng. J.*, JSCE, Vol. 43(4), 317–337.
- Serizawa, M., Uda, T., San-nami, T., Furuike, K., and Kumada, T. 2003. Improvement of contour line change model in terms of stabilization mechanism of longitudinal profile, *Coastal Sediments '03*, ASCE, 1–15.
- Serizawa, M., Uda, T., Suzuki, K., Maruyama, S., Takano, H., San-nami, T., and Ishikawa, T. 2009. Numerical simulation of rapid erosion of Seisho coast triggered by storm waves during Typhoon 0709, *Proc. Coastal Dynamics 2009*, Paper No. 93, 1–14.
- Uda, T., Serizawa, M., and Miyahara, S. 2018. Morphodynamic model for predicting beach changes based on Bagnold's concept and its applications, INTEC, London, UK, p. 188.
<https://www.intechopen.com/books/morphodynamic-model-for-predicting-beach-changes-based-on-bagnold-s-concept-and-its-applications>.